Vibrational properties of ultrathin PTCDA films on Ag(110)

F. S. Tautz,* S. Sloboshanin, and J. A. Schaefer
Institut für Physik, Technische Universität Ilmenau, P.O. Box 100565, D-98684 Ilmenau, Germany

R. Scholz
Institut für Physik, Technische Universität Chemnitz, D-09107 Chemnitz, Germany

V. Shklover, M. Sokolowski, and E. Umbach
Experimentelle Physik II, Universität Würzburg, Am Hubland, D-97074 Würzburg, Germany
(Received 18 October 1999; revised manuscript received 10 February 2000)

We have investigated 3,4,9,10-perylene-tetracarboxylic acid-dianhydride (PTCDA) films on the Ag(110) surface by High-resolution electron energy loss (HREEL) and Fourier transform infrared (FTIR) spectroscopy. X-ray photoemission spectroscopy, low-energy electron diffraction (LEED), and quadrupole mass spectroscopy were used to control thickness, composition, and order of the vacuum-sublimated PTCDA films. Taking advantage of the high surface sensitivity of HREELS, it is possible to clearly distinguish molecules in direct binding contact to the surface from those being in a PTCDA environment, because the spectra show differential peak shifts of the vibrational lines for the former molecules. To aid the interpretation of the spectra, discrete Fourier transform calculations of the vibrational frequencies of the free molecule were carried out. The results are in good agreement with the experimental values for the molecules in the multilayer and allow the identification of most of the experimental modes, if experimental information from off-specular HREELS measurements is taken into account. By the comparison of the calculated frequency spectrum with FTIR data it is possible to extract the effects of the intermolecular interaction on the vibrational spectra.

I. INTRODUCTION

Detailed knowledge about organic/inorganic interfaces is presently missing, partly because the interaction between large organic molecules and metal surfaces appears to be rather complex, and partly because large unit cells and numerous electronic or vibrational peaks make the analysis of experimental data very complicated. This stands in contrast to the general interest in such interfaces, since these largely determine the properties of optoelectronic devices based on molecular materials as an active component, such as thin-film transistors,[1,2] organic light-emitting devices (OLEDs),[3,4] and flat panel displays,[5] to name just a few. Although such devices, especially OLEDs, have attracted enormous activities in basic research as well as in industry, resulting in products on the market, the basic knowledge especially about the interfaces involved is still rudimentary. Therefore it is important and, considering the complexity, a challenge for surface science to improve our understanding about organic/inorganic interfaces.[6] In the present paper we do this by using vibrational techniques, which have been proven to yield a detailed insight into adsorbate properties in many cases, and by applying these techniques to the well-established and for applications relevant molecule 3,4,9,10-perylene-tetracarboxylic acid-dianhydride (PTCDA), here on the Ag(110) surface.[6–8]

The growth of PTCDA on metallic surfaces has been investigated by various surface-sensitive techniques, leading to some overall understanding of these layers and of the growth process. Highly surface-sensitive electron diffraction [low-energy electron diffraction (LEED)] patterns show a high degree of structural order and allow the symmetry determination of the various phases.[7–10] Real-space structural models could be deduced from LEED patterns and scanning tunnel microscope (STM) images of monolayer films.[7,8,11–13] More recently, electron diffraction with high resolution in *k*-space [spot profile analysis LEED (SPALEED)] investigations made it possible to study relaxed-vs-strained growth as a function of interface preparation and film thickness.[14] Electronic structure investigations by near-edge x-ray absorption spectroscopy (NEXAFS) (empty states) (Ref. 15) and by photoelectron spectroscopy (filled states)[16,17] demonstrated the chemisorptive nature of the bonding of the molecule to the surface by differential peak shifts of molecular orbitals. The molecular orientation on the surface is known from NEXAFS experiments with polarized synchrotron radiation, which show that PTCDA adsorbs in flat-lying geometry on most substrate surfaces.[6,15] As a result of these and similar investigations on various substrates it has been possible, in essence, to delineate three growth regimes whose realization depends on the strength of the molecule-substrate interaction.[6] True epitaxy is found only for those molecule-substrate combinations where the interaction is strong enough to enforce an epitaxial relationship between the substrate and the molecular lattices, but weak enough to allow a sufficient mobility of the molecules on the surface to prevent a hit-and-stick behavior during growth.

In this paper we investigate the vibrational properties of PTCDA on Ag(110). If, as mentioned above, chemisorption leads to differential peak shifts of the *electronic levels* of the molecule as a result of the formation of bonds between molecules and the surface, then the molecular geometry and/or the internal dynamics of the molecule should also be strongly affected by this rearrangement of the electronic wave func-

tions, leading in turn to frequency shifts of the *vibrational modes*. Unlike the assignment of electronic levels, the assignment of the well-separated lines in the *vibrational* spectrum is usually straightforward, especially in conjunction with theoretical calculations (despite the fact that the number of possible modes for a molecule with 38 atoms is rather large). Detailed information about the substrate-induced effects on the molecule can thus be obtained from the specific behavior of certain modes, whose eigenvectors are known from the calculations. This aim has motivated the present study, in which we have employed both inelastic electron scattering from surfaces [high resolution electron energy loss spectroscopy (HREELS)] and Fourier transform infrared reflection absorption spectroscopy (FTIRRAS) to record vibrational spectra. While both offer similar information about the vibrational modes of adsorbed molecules and thin molecular films, the advantage of HREELS over FTIR spectroscopy is the extremely high surface sensitivity of much less than 0.1 monolayer (ML) and the ready accessibility of the complete spectral range, effectively starting at approximately 20 cm^{-1} (2.5 meV) and extending into the eV range (electronic transitions). Since we are mainly interested in the vibrational spectra of molecules in direct binding contact with the surface, the ability to record spectra at submonolayer coverage is of great importance.

The paper is organized as follows: Section II will deal with experimental details of film preparation and measurements. In Sec. III we then turn towards a brief general description of the PTCDA/Ag(110) system. In Sec. IV the spectrum of thick (multilayer) films will be discussed, including experiments for the determination of mode polarizations. A comparison between calculated mode frequencies and measured spectra will be given in Sec. V, leading to our mode assignment. In Sec. VI we will discuss the influence of substrate bonding on the vibrational spectra. Finally, the paper closes with conclusions and an outlook in Sec. VII.

II. EXPERIMENTAL

The PTCDA layers were grown in an ultrahigh vacuum (UHV). We used PTCDA, which had been sublimation purified prior to loading into the Knudsen cell from which it was evaporated. Evaporation took place between 420 and 430 °C. At these temperatures, growth rates of 0.2 ML/min were achieved. The silver samples were cleaned in situ by the conventional procedure of repeated sputter-anneal cycles. For sputtering, the sample was bombarded with 1 kVAr^+ ions, yielding a target current of 10 μA at partial Ar pressures of ca. 2×10^{-6} torr. The annealing temperature was set to 700–800 K. This temperature was maintained for 30 min. Between the cycles the surface order was checked using low-energy electron diffraction (LEED), and the cleanliness of the surfaces was checked occasionally with core-level x-ray photoelectron spectroscopy (XPS) and HREELS. Once a sharp LEED pattern was observed, the initial cycling was terminated and the first PTCDA layer was grown.

Experiments were always carried out in the following sequence: HREEL spectra were recorded first, then LEED images were taken, and finally XPS spectra were measured. During LEED sessions, which could last up to 30 min, we did not observe any deterioration of the LEED patterns, indicating that electron bombardment has no significant impact on the film order. Similarly, no changes in the HREEL spectra during data collection on one film were observed, showing that the molecules themselves survive electron bombardment. Each film was grown onto a freshly prepared silver substrate. None of the films was grown on top of an earlier PTCDA film. In order to keep a possible beam damage caused by electron impact to a minimum, we used a low primary beam electron energy of 2.3 eV for all our HREEL spectra. The angle of incidence of the electrons in the HREELS experiment was set to 60° with respect to the surface normal.

Layer thicknesses were calibrated using a combination of quadrupole mass spectrometry (QMS), XPS, and LEED. During each evaporation the partial pressure of a fragment of the PTCDA molecule was monitored. This fragment occurs at 124 amu, corresponding to a doubly ionized PTCDA molecule from which 6 oxygen atoms and 4 C atoms (i.e., both anhydride groups) are abstracted. The fragmentation takes place during ionization in the QMS, as checked earlier in a separate UHV chamber equipped with a 1000-amu quadrupole. Unlike the background pressure, which also rose during the warmup of the closed Knudsen cell, the 124-amu signal was picked up *only* when the shutter of the Knudsen cell was open, rising by a factor of 30 to 40. Similarly, it could only be observed when the quadrupole was installed in direct line of sight with the orifice of the cell. We therefore were able to use this signal as an on-line control of the evaporation process. The signal was stored and integrated to give a measure of the total PTCDA exposure during any particular evaporation session. A good proportionality between the evaporation time and the integrated charge could be established.

Independent of the QMS monitoring just described, a direct measurement of layer thickness was performed with XPS. For each of the films, the signals of the Ag 3*d*, O1*s*, and C1*s* core levels were recorded with high resolution. The O1*s* and C1*s* signals showed the characteristic splittings due to differently bonded atoms in the molecule (chemical core-level shifts). Using a surface layer model, the attenuation of the Ag 3*d* and the increase of the C1*s* and O1*s* signal was quantitatively evaluated and converted into a layer thickness. While this procedure gives internally consistent relative thicknesses, the absolute thicknesses thus obtained depend on the value of the inelastic mean-free path (λ) of Ag 3*d* electrons on their way through the PTCDA layer. In accordance with the universal curve for inelastic mean-free paths through matter[18] we chose $\lambda = 14$ Å. For a monolayer of PTCDA on Ag(110) this yielded an effective layer thickness of 2.8 Å, which is in reasonable agreement with the spacing of 3.2 Å between the (102) planes in the PTCDA bulk structure.[19]

The absolute thickness calibration was finally established by LEED. The highest coverage at which the LEED pattern showed a sharp brick-wall pattern[8,9] without even the slightest hint of diffraction spots belonging to the herringbone structure, which occurs in the second layer (see Fig. 1, and discussion in Sec. III), was set to 1 ML. As the results of the present work will demonstrate, HREEL spectra themselves can be used as a very sensitive means to delineate the monolayer coverage. In this respect we find excellent consistency

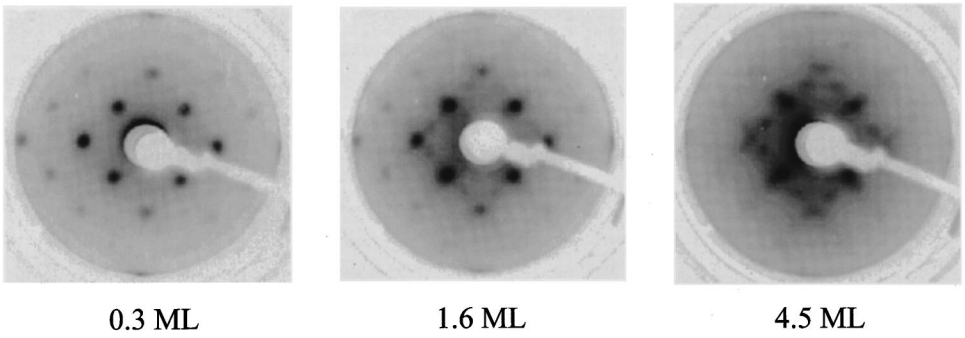

FIG. 1. LEED images of various PTCDA films on Ag(110). Beam energy: 14 eV. Thicknesses in monolayers (ML) are derived as described in the text. (a) Brick-wall structure; (b) brick-wall structure with additional spots corresponding to the herringbone structure of the second layer; (c) herringbone structure.

between the LEED XPS, and HREELS determinations of film thicknesses.

A final note concerning the convention for quoting frequencies: Throughout the paper, experimental frequencies are given in normal typescript as integer values, the accuracy being ± 1 cm^{-1} in the best cases. Theoretical frequencies, in contrast, are printed in italics.

III. PTCDA/Ag(110)

As pointed out in the Introduction, the main aim of the present study is the detailed description of the effect of the substrate bonding on the internal dynamics of the molecule. As a model system, which is well suited for this goal, we have chosen the flatly adsorbing PTCDA on the Ag(110) surface, since in this case the interaction between substrate and molecule leads to a specific ordering of the molecules in the first monolayer, which is not found in PTCDA bulk crystals, indicating a relatively strong binding of the molecule to the surface.[7] The effect of the chemical bonding should therefore also become apparent in the vibrational spectra.

The PTCDA monolayer on Ag(110) is a commensurate single-domain structure (apart from translational domains) with space group cmm, the so-called brick-wall structure (see Fig. 2). The corresponding LEED image is reproduced in Fig. 1(a). The nearly square unit cell of the PTCDA lattice is rotated by 43.3° relative to the unit cell of the silver lattice. It contains one molecule, the surface area per molecule being 141.4 Å^2. The angle between the two unit vectors of the PTCDA lattice is 86.7°, their length amounts to 11.9 Å. These structural data have been obtained from STM images.[7,8] The exact adsorption site of the PTCDA molecule on the silver lattice has been established by Ag-adatom manipulation in vicinity of PTCDA islands,[13] the adatoms serving as convenient markers of the Ag substrate lattice. Figure 2 shows the adsorption site of the PTCDA molecule thus determined.

In Figs. 1(b) and 1(c), which correspond to a coverage of 1.6 and 4.5 ML, respectively, one observes additional diffraction spots. These belong to molecules in the second and higher PTCDA layers. From the second monolayer onwards the flat-lying molecules order in a structure that is very similar to the (102) planes of the PTCDA bulk crystal structure.[19,20] In this plane the molecules are arranged in the characteristic herringbone pattern [two-dimensional (2D) space group $p2$], in which they are more densely packed than in the brick-wall structure. Moreover, in the bulk herringbone structure the molecules are slightly tilted out of the crystallographic (102) plane.[21] It is currently not known whether this is also the case for the second and higher layers grown on Ag(110). It is, however, certain that the in-plane structural parameters of quasiepitaxial films on silver differ slightly from the PTCDA bulk structure.[7] For PTCDA on Ag(111) it is known that the relaxation of the films to the exact crystal structure of bulk PTCDA occurs only at low temperatures for a specifically prepared incommensurate monolayer.[14]

IV. VIBRATIONAL SPECTRA OF THE PTCDA MULTILAYER

An isolated PTCDA molecule belongs to the symmetry group $D_{2h}(mmm)$. This group has only one-dimensional representations. Accordingly, all vibrational modes of the molecule are necessarily nondegenerate. The molecule has 108 internal degrees of freedom. 46 of its normal modes are infrared active (representations B_{1u}, B_{2u}, B_{3u}), 54 are Raman active (representations $A_g, B_{1g}, B_{2g}, B_{3g}$), and eight modes are silent (representation A_u).[22]

The scattering geometry of the present experiments is

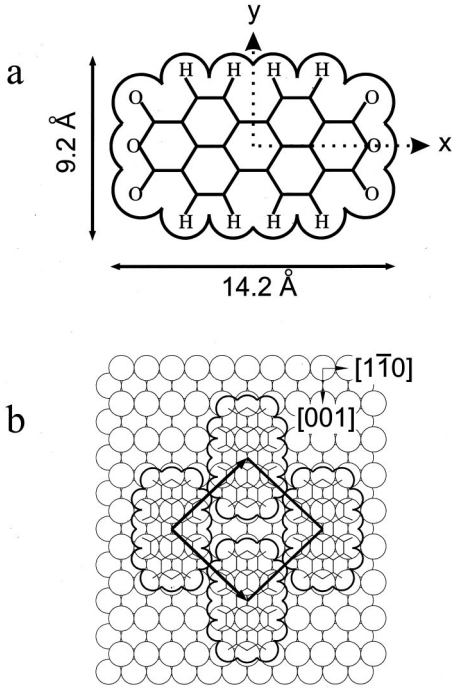

FIG. 2. (a) Chemical structure formula of the PTCDA molecule. x and y axes of the molecule are indicated. (b) Model of the PTCDA brick-wall structure on Ag(110). Plot reproduced from Ref. 7. Adsorbate unit cell and substrate directions given by arrows.

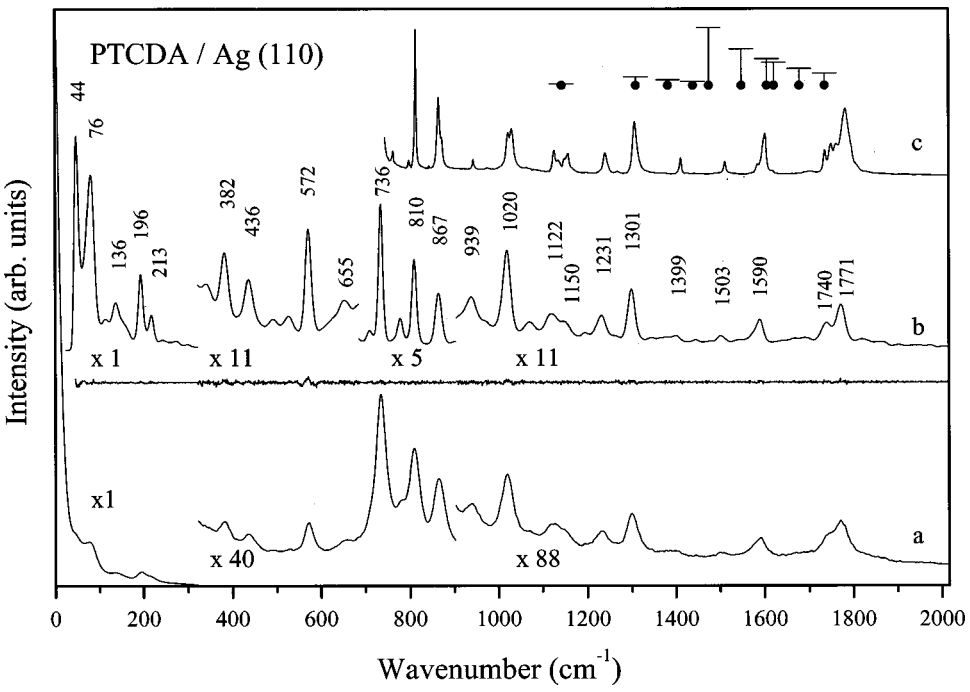

FIG. 3. PTCDA multilayer on Ag(110). (a) HREEL spectrum of 4.5 ML, (b) deconvoluted HREEL spectrum of 4.5 ML, including residual, (c) FTIR spectrum (grazing incidence, *p* polarization) corresponding to more than 10 ML PTCDA on Ag(111). (b) Frequency labels in cm^{-1} have been included for the stronger peaks that are also clearly visible in the as-measured data of (a). Vertical bars correspond to relative intensities of possible multiple losses, made up from the peaks at 572, 736, 810, and 867 cm^{-1} (see text). The vertical bars give the relative intensity of all twofold combination peaks containing the modes at 572, 736, 810, and 867 cm^{-1} as fundamentals.

such that the intersection of the scattering plane with the surface is rotated approximately 3° away from the short axis of the molecule in Fig. 2(b). The scattering plane thus almost corresponds to a mirror plane of the surface molecule. The angle of incidence of the electrons in this scattering plane was 60° against the surface normal.

A. Specular scattering geometry

Figure 3(a) shows a HREEL spectrum of a PTCDA multilayer on the Ag(110) surface. The coverage has been determined as 4.5 ML by the method described in Sec. II. Apart from the as-measured data, the figure also contains a deconvoluted spectrum, which has been obtained by a deconvolution routine[23,24] [Fig. 3(b)]. The quasielastic peak has been used as the instrument function for the deconvolution. The residual, i.e., the difference between the raw data and the convolution of the object function [Fig. 3(b)] with the instrument function is also plotted in between the two curves. As mandatory for a successful deconvolution, the residual contains mostly noise contributions. The deconvolution corresponds to a resolution enhancement by approximately a factor of 3, yielding a final resolution of ~6 cm^{-1}. Furthermore, an FTIR spectrum for a much thicker film (>10 ML) on Ag(111) has been plotted for comparison [Fig. 3(c)]. It turns out that for PTCDA multilayers with thicknesses above ~3 ML there is no difference in the HREELS spectra recorded on Ag(110) and Ag(111), such that a direct comparison between the spectra in Figs. 3(a), 3(b), and 3(c) is possible. In the frequency range above 800 cm^{-1} one observes an excellent overall agreement between the FTIR spectrum and the resolution-enhanced spectrum, as far as the peak positions are concerned. Even some very small features in the deconvoluted object function have counterparts in the FTIR spectrum. Moreover, the small peaks in Fig. 3(b) at 716 and 781 cm^{-1}, the latter of which is not observed in Fig. 3(c) are nevertheless real and will be discussed in more detail in Sec. VI. The HREELS deconvolution procedure, however, misses certain peak splittings which are present in the FTIR spectrum of Fig. 3(c): 1018/1026 cm^{-1}, 1122/1132/1146/1153 cm^{-1}, and 1731/1745/1756/1778 cm^{-1}. Similarly, the peak at 867 cm^{-1} in Fig. 3(c) has a shoulder. The origin of this peak splitting will be discussed in Sec. V.

In electron energy loss spectroscopy it is possible to excite multiple and combination losses. It is therefore necessary to check whether any of the modes that are observed in the spectra of Fig. 3 are due to such multiple scattering events. Judging from the frequencies alone, the modes at 213, 572, 810, 1020, and 1301 cm^{-1} could be due to multiple or combination loss events, since they fall within 2 cm^{-1} of combinations of other frequencies present in the spectrum. However, in all of these cases the intensity of the modes is inconsistent with their alleged origin as combination modes. In the case of the 572 and 1301 cm^{-1} modes, one of the contributing fundamentals is considerably *weaker* than the alleged combination, which rules out this interpretation. For the modes at 810 and 1020 cm^{-1} one can construct a new combination from one of the fundamentals and a third mode, which is stronger than the other fundamental; since this new combination is *not* found in the spectrum even though it should be stronger than the original alleged combination loss, this again rules out the interpretation of the 810 and 1020 cm^{-1} as combinations. Finally, for the modes at 212 and 1020 cm^{-1} an inconsistency between the symmetry of the two contributing fundamentals and the alleged combination proves that these modes are not combination losses. (For the determination of the symmetries of the various modes, see below in this section and in Sec. V.) To graphically illustrate the fact that also the high energy part of the spectrum is not shaped by multiple or combination losses, we have included bars in Fig. 3 that give the relative intensity of all twofold combination peaks containing the modes at 572, 736, 810, and 867 cm^{-1} as fundamentals. After careful analysis of the spectra in Fig. 3 one can thus conclude that all the major modes observed are fundamentals. In fact, we will show in Sec. V that each can be attributed to a calculated normal mode frequency.

Comparing Figs. 3(b) and Fig. 3(c) one observes good agreement of relative peak intensities in the respective spectra. This points to the fact that in both cases the physical quantities determining the (relative) intensities are the same. While in infrared spectroscopy intensities are *always* proportional to the squared dipole matrix element, in HREELS there is an additional scattering mechanism, namely, impact scattering, the cross sections of which are unrelated to dipole matrix elements. From the similarity in the relative intensities of spectra in Figs. 3(b) and 3(c) we can conclude that *all* the modes visible in the HREEL spectrum in Fig. 3(a) are dipole excited. However, close inspection reveals that the principal lines above 900 cm^{-1} are approximately a factor 2 weaker in HREELS as compared to FTIR. Partly, this may be due to the less effective resolution enhancement for the weaker peaks above 900 cm^{-1}, leaving them broad and small. Moreover, the gradual falloff of intensity with increasing loss energy as compared to FTIR is related to falling analyzer transmission. We have also evaluated HREEL spectra recorded at 3.5 and 11 ML coverage in exactly the same way as in Fig. 3(b), and we find that with increasing layer thickness certain modes, namely, the modes at 382, 436 cm^{-1} and all modes above 900 cm^{-1}, are enhanced in comparison with the modes at 572, 736, 810, and 867 cm^{-1}, while the relative intensities of the latter modes are identical for all film thicknesses.

These observations can be naturally explained in the framework of the surface selection rule if the peaks at 382, 436 cm^{-1}, and above 900 cm^{-1} are assigned to parallel polarized modes while the strong modes at 572, 736, 810, and 867 cm^{-1} are assumed to be $B_{1u}(z)$ modes: In dipole scattering *from metallic surfaces*, dynamical dipoles oriented parallel to the surfaces are completely screened by their image charges, such that parallel polarized modes are not excited by this scattering mechanism. In contrast, dynamical dipoles oriented normal to the surface are enhanced by a factor of 2 by their image dipole. In essence this selection rule is also valid in infrared spectroscopy (grazing incidence, *s* polarization); however, the FTIR spectrum reported in Fig. 3(c) corresponds to a film in excess of 10 ML.

Two inferences can thus be drawn from the observed strengthening of the mentioned modes at 382, 436 cm^{-1}, and above 900 cm^{-1} with increasing layer thickness. First, we observe *the gradual reduction of the screening of the parallel dynamical dipole moments by the underlying substrate (often referred to as surface selection rule) as the PTCDA layer thickness is increased*. Second, this behavior of the peak intensities gives us a first hint that the modes at 382, 436 cm^{-1} and above 900 cm^{-1} are all polarized in the plane, i.e., they belong to the representations $B_{1u}(x), B_{2u}(y)$. This conclusion is confirmed both by off-specular HREELS measurements, which will shortly be discussed, and by theoretical calculations. Two mechanisms are conceivable for the observed breakdown of the surface selection rule: First, the dielectric PTCDA layer suppresses the influence of the image charges surprisingly effective, and second, the surface selection rule as such remains valid while the orientation of the molecules slowly relaxes from the strictly flat-lying geometry (which is enforced in the monolayer by the presence of the surface) towards the structure of bulk PTCDA in which the molecules are slightly tilted around their diagonal out of the layer planes.[21]

B. Off-specular scattering geometry

While the mode intensities discussed in the previous paragraph give a first indication of mode polarizations, there is of course a more direct way to determine these, namely, conducting HREELS experiments in off-specular scattering geometry. Under these conditions the otherwise dominating dipole scattering mechanism is strongly suppressed, with the result that all modes are almost exclusively excited in the impact scattering mechanism, which in the present case is considerably weaker. Dipole-inactive modes become therefore discernable in the spectrum, with intensities now comparable to the intensities of the dipole active modes. After what has been said in the previous paragraph concerning the screening of parallel dipole moments, it is obvious that in the present case a clear-cut experimental distinction between *x*- or *y*-polarized modes on the one hand and *z*-polarized modes on the other remains restricted to extremely thin layers. For this reason, we have carried out an HREELS experiment with 17° off-specular detection on a submonolayer PTCDA film on Ag(110), so that one can be sure that the screening of parallel dipoles works as strictly as possible. The results are displayed in Fig. 4. For reference, the multilayer spectrum of Fig. 3 has been reproduced in Fig. 4.

When using submonolayer spectra with the purpose to investigate the polarization of multilayer modes, there is, however, a slight complication, as for the molecules in the first monolayer the symmetry breaking due to the presence of the substrate surface leads to the potential appearance of modes with symmetries other than $B_{1u}(x)$, $B_{2u}(y)$, or $B_{3u}(z)$ even in the *dipole* spectrum. On surface adsorption the symmetry group of the molecule is reduced from D_{2h} for the free molecule to at most C_{2v} [cf. Fig. 2(b)], due to loss of inversion and related symmetries at the surface. Of the non-IR-active representations of D_{2h}, the A_g representation projects onto the totally symmetric A_1 representation of the C_{2v} group of the surface-bound molecule. Corresponding modes become not only infrared active, but also allowed according to the surface selection rule. If the high-energy modes in Fig. 4(c) (1231 cm^{-1}, 1259 cm^{-1}, 1325 cm^{-1}, and 1569 cm^{-1}) are indeed excited in the dipole scattering mechanism, a notion which is supported by their relatively strong intensity in the submonolayer dipole spectrum compared to the other modes above 900 cm^{-1} in Fig. 4(c) (dashed lines in Fig. 4), then these modes must have A_g (parent molecule)/A_1 (surface-bound molecule) symmetry.

Comparing the multilayer with the submonolayer in specular detection, one observes dramatic differences. Some of these differences are a direct result of the strict validity of the surface selection rule for the submonolayer, e.g., the strongly reduced scattering intensity above 900 cm^{-1}. Accordingly, in the submonolayer off-specular experiment [Fig. 4(b)] modes that are detected in the multilayer in the frequency range 900 to 1650 cm^{-1} appear strongly enhanced relative to the corresponding submonolayer dipole spectrum [Fig. 4(c)], albeit with different intensities since they are now excited by the impact scattering mechanism (dotted lines in

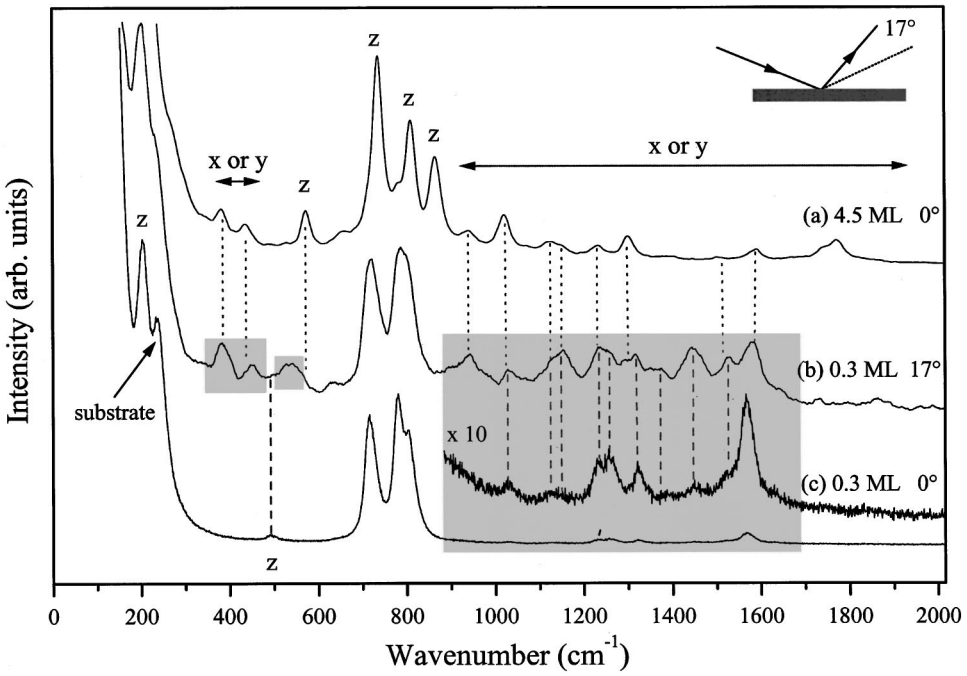

FIG. 4. Comparison between specular (bottom, c) and off-specular (middle, b) HREELS data for the submonolayer film of 0.3-ML thickness. The specular data of the 4.5-ML film (top, a) are the same as in Fig. 3. *x*, *y*, and *z* labels denote the polarization of the respective modes.

Fig. 4). The enhancement factors of these modes relative to the elastic peak are in the range 10 to 60. This is a conclusive proof that these modes are in-plane polarized. Similarly, the modes at 382 and 436 cm^{-1} are parallel polarized.

The modes between 500 and 600 cm^{-1} appear strongly in the off-specular spectrum, but not in the specular monolayer spectrum. Apparently these modes, while having a large impact scattering cross section, have a very small dipole matrix element. Alternatively, these could be modes belonging to any other representation of the group of the parent molecule, except for the B_{1u} (*x*-like) representation, since in the present off-specular impact scattering geometry a remnant selection rule applies (see below). Similar behavior is found for a few modes above 900 cm^{-1}, e.g., the mode at 1450 cm^{-1} [Fig. 4(b)]. In contrast, the modes in the frequency range 700 to 900 cm^{-1} have clearly *z* symmetry, since their enhancement factors relative to the elastic peak are between 2 and 3, while the elastic peak itself falls off by a factor 100. Similarly the mode at 204 cm^{-1} has *z* symmetry. For the modes with still lower frequency, the polarization can only be conjectured by comparison with theory (cf. Sec. V).

Figure 4 clearly shows that in the 700 to 900 cm^{-1} frequency range there are significant differences between multilayer and monolayer spectra that cannot be explained by any argument based on selection rules, since for the monolayer the specular (dipole) and the off-specular (impact) spectrum are identical in this frequency range. In Sec. VI we will look in more detail at these coverage-dependent frequency shifts.

There are two modes whose behavior appears to be specific. First, the weak *z* mode at 494 cm^{-1} (not enhanced under off-specular detection) is not observed in the multilayer spectrum. Meanwhile the multilayer spectrum shows a mode at 572 cm^{-1}, which is neither present in the dipole nor impact spectrum of the monolayer. On the basis of Fig. 4 the polarization of the latter mode is therefore ambiguous. However, it was mentioned already in the discussion of Fig. 3 that the layer-thickness-dependent relative intensity reveals this mode as being *z* polarized. The behavior of these modes will be discussed in more detail in Sec. VI.

V. MODE ASSIGNMENTS

In order to aid our interpretation of the complex vibrational spectra we have theoretically calculated the vibrational frequencies for an isolated molecule. To this purpose, density functional calculations of the electronic structure of the molecule were used to generate the equilibrium structure of the molecule and the vibrational eigenfrequencies and eigenvectors in turn. We used two different basis sets for these DFT calculations, one being an optimized tight binding set,[25,26] the other the more time consuming 6-31 G set from the GAUSSIAN98 package[27] (B3LYP functional[28]). The results of the calculations are displayed in Fig. 5 and in Table I, along with experimental data. Figure 5 contains all of the 46 calculated IR active frequencies (basis set 6-31 G) and the resolution enhanced 4.5-ML PTCDA/Ag(110) spectrum. The height of the columns gives the predicted infrared intensity. The overall agreement between the calculated and the experimental spectra is excellent as far as the frequencies are concerned, not always satisfactory as far as the intensities are concerned.

Most importantly, the upper limit for out-of-plane modes at ~900 cm^{-1} is correctly reproduced. In the low-frequency region up to about 150 cm^{-1}, the agreement between calculation and experiment is less convincing than at higher loss energies. This is, however, not surprising, since in this energy range one expects external modes in addition to the internal modes of the free molecule. Moreover, these frustrated rotations and translations will couple to the low-frequency internal modes in which large parts of individual molecules move as rigid units. This will lead to new modes of mixed character, which have no counterpart in the calculated spectrum.

Strong out-of-plane modes are predicted at *591*, *732*, *803*, and *889* cm^{-1}. This reproduces the positions of the four

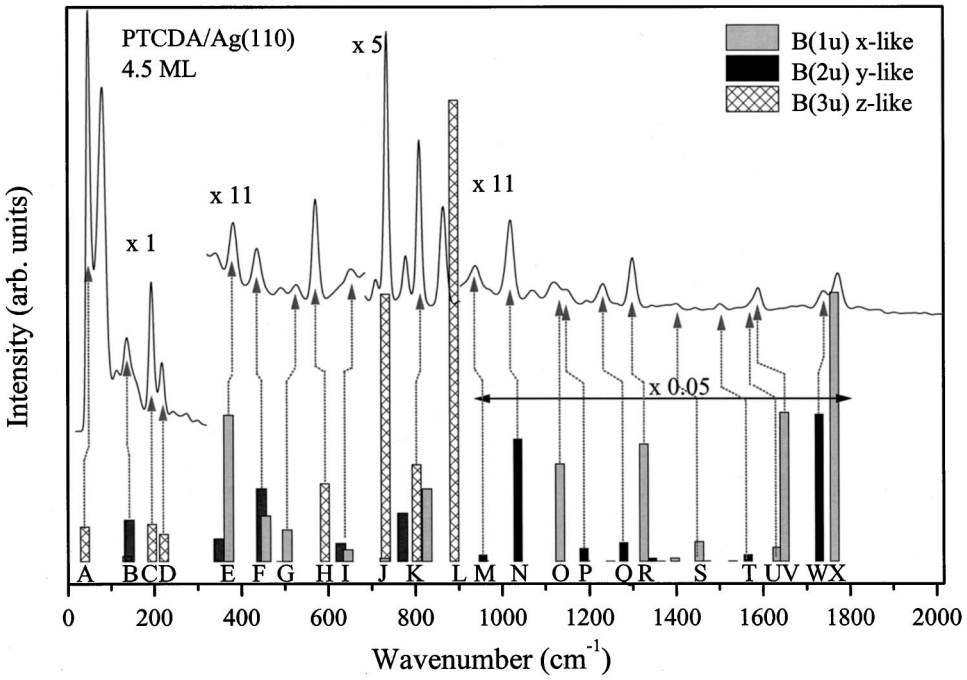

FIG. 5. Comparison between the resolution-enhanced (deconvoluted) multilayer spectrum (4.5 ML) of Fig. 3 and all calculated IR active mode frequencies (basis set 6-31G, see text). Representations: B_{1u} (x-like), B_{2u} (y-like), B_{3u} (z-like), the x axis being the long axis of the molecule. Bars appear at the calculated energy positions, the height (in arbitrary units) is proportional to the calculated infrared intensities. From 900 cm^{-1} onwards the bars have been reduced by a factor 20 in height. From 300 cm^{-1} onwards, the data have been vertically displaced. Scaling factors of the experimental data relative to the low-energy regime are given. Arrows give the most important assignments that can also be found in Table I.

strongest z modes with accuracy within 3%. In the region above 900 cm^{-1}, each of the strong experimental peaks can be assigned to an in-plane mode with strong dipole matrix element within an error of less than 4%. Only in the range from 1380 to 1580 cm^{-1} it is impossible to assign the experimental modes to calculated frequencies with certainty. In Fig. 5, we have reduced the calculated infrared activity of the calculated modes above 900 cm^{-1} by a factor of 20. In the regions above and below this threshold the strongest calculated modes more or less correspond to the strongest experimental modes. However, if intensities are compared across this threshold the high-frequency modes are too weak by an order of magnitude. This observation, which also holds for the FTIR spectrum in Fig. 3, is related to the nearly parallel orientation of the molecules to the surface, as discussed in the previous section.

An eigenvector analysis reveals the detailed nature of the modes. These have been included in Table I. Both calculations yield very similar eigenvectors. Additionally, the relative quadratic displacements from the DFT calculation in the optimized tight-binding basis are listed in order to characterize the modes. The out-of-plane modes below 200 cm^{-1} involve both the perylene core of the molecule (skeleton modes) and the anhydride groups. These modes are characterized by simple node-line patterns. With increasing frequency the node-line patterns become more complicated, while the contribution of the anhydride group is decreasing. The highest out-of-plane vibrations are the HC-CH wagging at 867 cm^{-1} and the HC-CH twisting calculated at *1030* cm^{-1}, which is, however, not observed because its dipole activity is near zero. The low-frequency in-plane modes involve C-O-C, C-C-O, and C-C=O bending vibrations in the anhydride group. The principal C-O-C stretch vibrations occur at 1020 and 1122 cm^{-1}. C-H bending in-plane vibrations extend from 1000 cm^{-1} up to 1400 cm^{-1}. Above 1150 cm^{-1} and up to 1630 cm^{-1} C-C stretching elongations are additionally contained in the eigenvectors, especially above 1400 cm^{-1}. The highest frequencies belong to the C=O stretch modes (calculated at *1729* and *1764* cm^{-1}, vs experimental 1740 and 1771 cm^{-1}) and the C-H stretch modes (*3232-3260* cm^{-1} or *3168-3190* cm^{-1} calculated, observed at 2990 to 3180 cm^{-1}).

The comparison with the calculated spectra also yields the exact polarization of the multilayer modes. As far as the distinction between out-of plane and in-plane modes is concerned, the calculations are in excellent agreement with the experiment, as discussed in Sec. IV. Given the present scattering geometry, the off-specular experiment allows the distinction between in-plane modes of x-(B_{1u}) and y-(B_{2u}) polarization: The scattering plane is parallel to the short (y) axis of the molecule and thus coincides with the respective mirror plane of the surface-bound molecule. As a result, we are only able to observe modes in impact scattering, which are even under the reflection at this mirror plane, e.g., B_{2u} modes, due to the operation of a remnant selection rule (time-reversal symmetry).

According to the assignment in Table I, the modes at 382 cm^{-1} and 436 cm^{-1} have x-like and y-like symmetry, respectively. Due to the impact scattering selection rule one expects to observe only the mode at 436 cm^{-1} in the off-specular experiment documented in Fig. 4(b). As evident from Fig. 4(b), however, we also observe the mode at 382 cm^{-1}. The reason for this apparent contradiction is the fact that very close to the respective dominating x and y modes, respectively, modes of opposite character can be found at calculated frequencies of 348 cm^{-1}(y) and 455 cm^{-1}(x), see also Fig. 5. The experimentally observed peaks should thus correspond to ''mixed'' modes, and the mixed character is nicely borne out by absence of symmetry specificity in the off-specular scattering experiment. For the modes above 900 cm^{-1}, there is in fact a general tendency that modes with y-symmetry are more prominent in the spectrum of Fig. 4(b), in agreement with the impact-scattering selection rule.

We will now briefly mention assignments that have been previously published for the PTCDA molecule. Akers *et al.*[22] have carried out Raman and IR spectroscopy on 200-nm

TABLE I. The table contains the frequencies of all normal modes found in this work. The first column includes in brackets those very weak features that are clearly seen only in the resolution-enhanced HREEL spectrum but for which there exists a corresponding line in the FTIR spectrum (see column 2). In the first column, the letter *z* refers to experimentally determined out-of-plane polarization, while *p* refers to experimentally determined in-plane polarization. Column 3 gives DFT frequencies based on the B3LYP 6-31G basis set; column 4, DFT frequencies based on the optimized tight-binding basis. The assignments in column 3 correspond to those marked by arrows in Fig. 5, capital letters have been used for better access. Calculated mode polarizations are given in brackets along with the calculated frequencies. Columns 5 and 6 contain information about the respective eigenvectors taken from the calculations in columns 3 and 4, respectively. Column 7 contains the set of FTIR data by Alkers *et al.* (Ref. 22).

HREELS multilayer cm^{-1}	FTIR multilayer cm^{-1}	Theory I cm^{-1}	Theory II cm^{-1}	Displacement (theory I and theory II)	Type (Δr^2) (theory II) C:H:O %	Akers IR cm^{-1}
44		38 (*z*) *A*	36 (*z*)	short-axis folding I	47:21:32	
76		-	111 (*z*)	O=C-O twist/long-axis folding I	06:09:85	
136		137 (*y*) *B*	136 (*y*)	DiAn vs perylene shear	40:22:38	
196 (*z*)		194 (*z*) *C*	174 (*z*)	molecule bucking/long-axis folding II	30:69:01	
213		222 (*z*) *D*	195 (*z*)	short-axis folding II	63:29:09	
382 (*p*)		371 (*x*) *E*	362 (*x*)	C-C=O, C-O-C bend	16:22:62	
436 (*p*)		446 (*y*) *F*	427 (*y*)	C-C-O, C-C=O bend	47:40:13	438
(494) (*z*)		(492) (*z*)	444 (*z*)	HC-CH twist	24:76:00	
527 (*p*)		504 (*x*) *G*	507 (*x*)	C-C-O bend (C-C=O, C-O-C)	39:38:23	503
572 (*z*)		591 (*z*) *H*	531 (*z*)	long-axis folding III	94:01:05	572
						603
655 (*p*)		628 (*y*) or 645 (*x*) I	625 (*y*) 652 (*x*)	C-C=O, C-C-O bend or C-O-C, C-C-O bend	59:35:07	641
						668
736 (*z*)		732 (*z*) *J*	695 (*z*)	C-C ripple	67:19:04	734
	759					759
	794					
810 (*z*)	809	803 (*z*) *K*	769 (*z*)	C-C ripple	66:33:01	809
	860					862
867 (*z*)	867	889 (*z*) *L*	818 (*z*)	HC-CH wagging	03:97:00	
939 (*p*)	939	955 (*y*) *M*	983 (*x*)	C-O-C stretch, C-C-O bend, C-H bend	51:43:06	938
(972) (*p*)	972					
1020 (*p*)	1018	1036 (*y*) *N*	1052 (*y*)	C-O-C stretch, C-H bend	40:38:22	
	1026					1025
(1070)	1060					1059
1122 (*p*)	1122	1133 (*x*) *O*	1117 (*x*)	C-H bend, C-O-C stretch	04:95:01	1122
	1132					
1150 (*p*)	1146	1187 (*y*) *P*	1147 (*x*)	C-H bend, (C-O-C stretch)	14:85:01	1150
	1153					
(1195) (*p*)	1194	1190 (*x*)	1189 (*y*)	C-H bend	15:85:00	
1231 (*p*)	1236	1278 (*y*) *Q*	1259 (*y*)	C-H bend, C-C stretch, (C-O-C stretch)	28:71:01	1234
(1264) (*p*)	1263					1266
1301 (*p*)	1302	1325 (*x*) *R*	1304 (*x*)	C-H bend, C-C stretch, (C-O-C stretch)	10:90:00	1300
1399 (*p*)	1406	1453 (*x*) *S*	1429 (*x*)	C-C stretch, C-H bend	38:62:00	1406
1503 (*p*)	1507	1565 (*y*) *T*	1552 (*y*)	C-C stretch, C-H bend	34:66:00	1506
	1580	1632 (*x*) *U*	1623 (*x*)	C-C stretch, no DiAn	49:51:00	
1590 (*p*)	1597	1649 (*x*) *V*	1646 (*x*)	C-C stretch, no DiAn	63:37:00	1594
	1613					
(1693) *p*)	1699					
	1731					1731
1740 (*p*)	1745	1729 (*y*) *W*	1690 (*y*)	C=O stretch	68:00:32	1744
	1756					1756
1771 (*p*)	1778	1764 (*x*) *X*	1717 (*x*)	C=O stretch	69:03:28	1772

films evaporated onto quartz and KBr. For comparison, their observed frequencies are also included in Table I. The authors assign their frequencies of 438, 572, 641, 734, 759, 809, 862, and 938 cm^{-1} to out-of-plane modes, in agreement with our data except for the modes at 438 and 938 cm^{-1}, for which we have presented conclusive evidence (both theoretical and experimental) that these modes are in-plane modes. For the in-plane modes above 1000 cm^{-1} Akers *et al.* suggest some assignments, albeit without presenting any supporting evidence. Alternative assignments, which partly contradict each other and those of Akers *et al.*, have been suggested by Murakami *et al.*,[29] Kamo *et al.*,[30] and Fuchigami *et al.*,[31] again without detailed argument.

It was mentioned in Sec. IV that the FTIR spectra of the multilayer show characteristic splittings for certain lines: 1018/1026 cm^{-1}, 1122/1132/1146/1153 cm^{-1}, and 1731/1745/1756/1778 cm^{-1}. Similarly, the peak at 867 cm^{-1} in Fig. 3(c) has a shoulder. Comparing to the calculations for the free molecule, we are now in a position to discuss the origin of these splittings. According to Fig. 5, for each of these *twofold*- or *fourfold*-split modes, only *one* or *two* IR active modes, respectively, are expected in the free molecule. Apparently, for these particular modes a frequency doubling takes place once the molecules condense into a thin film. We note that both in the PTCDA bulk structure and the quasiepitaxial film structure investigated here the unit cell contains two molecules (herringbone structure).[7,19,20] Via the dipole-dipole interaction or any other interaction (e.g., steric interaction), this leads to the observed duplication of mode frequencies, because these two molecules are not equivalent anymore (Davydov splitting). As expected, this interaction affects primarily those modes that have a large contribution located on the periphery of the molecule, i.e., in order of ascending frequency, the HC-CH wagging mode, the C-O-C stretching mode, the C-H bending mode and the C=O stretching vibrations (cf. Table I). In fact, the remarkable coincidence of mode character and splitting independently confirms our mode assignments. For example, we draw attention to the fact that the mode at 809 cm^{-1}, which we assign to a skeleton mode and which should thus not show the frequency doubling, is indeed much sharper than the HC-CH wagging mode at 867 cm^{-1}, which has a shoulder on the high frequency side.

VI. VIBRATIONAL SPECTRA OF PTCDA SUBMONOLAYERS

In the discussion of Fig. 4 it has already become apparent that there are strong differences between the multilayer and monolayer spectrum of PTCDA on Ag(110). In this section we argue that these differences are the result of the interaction of the molecule with the substrate. In order to study this issue, we have carried out a series of experiments on PTCDA layers with increasing thicknesses. The results are displayed in Fig. 6. One observes the existence of three groups of modes. Some modes exist both in the (sub)monolayer and in the multilayer at the same frequencies (group b). A second group is also present at all layer thicknesses, but their respective frequencies are shifted (group a). Third, some modes are present only in the multilayer (group c).

As mentioned before, specular dipole spectra of PTCDA submonolayers on Ag(110) can in principle show all modes, which are totally symmetric under the C_{2v} group of the surface-bound molecule. These are all modes belonging to the A_g and B_{3u} representations of the parent molecule. (Of these two, only B_{3u} modes are IR active in the free molecule and thus in the multilayer films.) When assigning the experimentally observed submonolayer modes from dipole scattering experiments, one thus has to compare with both the IR active B_{3u} and the Raman active A_g modes of the parent molecule. However, due to the modification of the molecule by the surface one will have additional frequency shifts for both types of modes, so that the assignment to calculated frequencies of the free molecule is not always unambiguously possible. In Table II we have listed both the experimental Raman A_g frequencies of PTCDA multilayers[26] and the experimental B_{3u} multilayer modes from Table I in comparison with the major (i.e., dipole excited) experimental submonolayer modes from the specular spectra. Each monolayer frequency is given opposite to the nearest multilayer mode, generally without implying a correspondence. Apart from the group of three monolayer modes between 700 and 810 cm^{-1}, which clearly correspond to the group at 736 to 786 cm^{-1} in the multilayer, the correct assignment of the submonolayer modes is not unambiguous and will probably require calculations for the surface-bound molecule. This is demonstrated by the inset to Fig. 6, which presents the magnified spectrum in the frequency range from 1150 to 2000 cm^{-1}, together with the experimental Raman modes from[26], which are also contained in column 5 of Table II. Although there is some agreement between the submonolayer HREELS data and the multilayer Raman data around 1600 cm^{-1}, the other modes cannot be assigned with any certainty. In particular, we note that the breathing C=O stretch mode is missing from the HREELS data. This observation will be discussed in more detail in Sec. VI B below.

A. C-C skeleton and HC-CH wagging modes in the frequency range 700 to 900 cm^{-1}

The most striking differences appear for the modes in the range 700 to 900 cm^{-1}. In Fig. 7 we have zoomed into this frequency range and also added the results of a peak-fitting procedure. For this peak fitting, the profile of the elastic peak plus some additional contributions from inhomogeneous broadening were applied to the component lines. Before the fitting a cubic background was subtracted in the displayed frequency range. In total six component lines are necessary to fit the spectra. This number corresponds to the number of separate features in the spectra discernible by the eye, as can also be deduced from the deconvoluted spectrum displayed in Figs. 3 and 5. The agreement between the deconvolution procedure and the conventional peak fitting with respect to the peak positions of the component lines is excellent. We note that the energy position of the individual component lines were left free to adjust during the fitting process, as well as their intensity. Only the line width was kept fixed. Nevertheless, Fig. 8(a) demonstrates the constancy of the line positions for all six spectra. This is strong evidence that the spectra in the range 700 to 900 cm^{-1} are indeed the result of the contribution of exactly six distinct modes, independent of the film thickness.

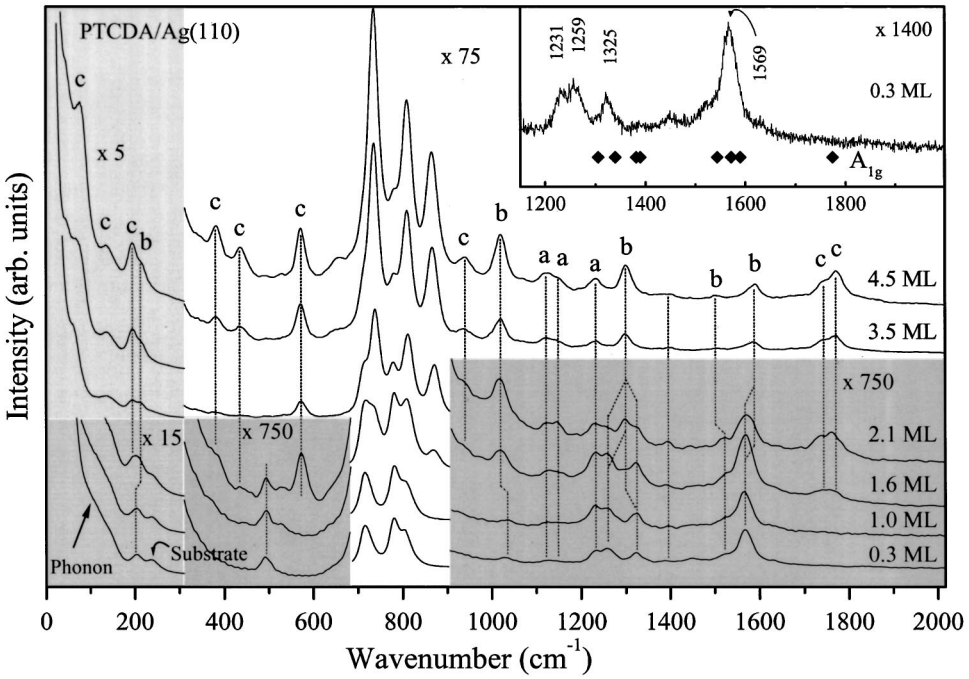

FIG. 6. Overview HREEL spectra of PTCDA on Ag(110) for various layer thicknesses in the range 0.3 to 4.5 ML. Shaded areas denote identical amplification factors relative to the elastic peak. (a), (b), and (c) denote different types of mode behaviors. (a) Modes are present both in mono- and multilayer, but shifted in frequency. (b) Modes are present both in mono- and multilayer at the same frequency. (c) Modes are present only in multilayer spectra. Inset: Magnified section of the 0.3-ML spectrum. Diamonds give the experimental Raman shifts of breathing A_g modes of PTCDA multilayers.[26]

Each of the spectra at the highest (4.5 ML) and the lowest coverage (0.3 ML) are dominated by only three lines. For intermediate coverages, a superposition of these two sets of three modes is observed. It is important to note that none of the lines continuously shifts in frequency. Rather, the intensities are gradually redistributed between the two sets. This can be seen most clearly in Fig. 8(a) where the size of the respective symbols gives a qualitative indication of the strength of the mode, and in Fig. 8(b) where the area under the component lines has been plotted versus the coverage. Obviously the molecules in the first monolayer, which are in direct binding contact with the silver substrate, are modified, and as a result each of the three strong *z* modes considered here is frequency shifted. In contrast, from the second layer onwards no further modification of the molecules is distinguishable. The monolayer modes occur at 716, 781, and 808 cm^{-1}, while the multilayer modes are found at 736, 810, and 867 cm^{-1}. Apparently the mode at 808/810 cm^{-1} appears for both mono- and multilayers. Whether this is due to an accidental degeneracy between a monolayer mode and a *different* multilayer mode or whether the mode at 810 cm^{-1} does not shift at all cannot be decided from the information given so far. In any case, the frequency shifts between monolayer and multilayer are differential, i.e., different modes shift by different amounts (see Table I). This is also true for all other modes labeled ''a'' in Fig. 6 and points towards a true molecular modification (electronic and/or geometric) as the origin of the effect. One can at this stage only speculate about the nature of the modified electronic or geometric structure induced by the chemical bonding to the substrate.

We have also carried out a 17° off-specular measurement for the 1.6-ML sample. The result is displayed in Fig. 8(c). It is obvious that the relative intensities of the six contributing modes change when the scattering mechanism is varied. We have fitted the off-specular spectra at 0.3 ML and 1.6 ML in exactly the same way as was previously done for the specular spectra (Fig. 7) and used the results to calculate off-specular enhancement factors for each of the modes, i.e., the factors by which the respective mode is enhanced relative to the elastic peak when switching from specular to off-specular detection. Modes with a large impact scattering cross section should have large off-specular enhancement factors. If the impact scattering cross section was zero, then the enhancement factor would be unity. For an impact scattering cross section of the same size as the dipole scattering cross section in specular geometry, the enhancement factor would effectively be half the ratio of the respective elastic peaks. In principle, the enhancement factors can thus be used to identify modes by their impact scattering cross sections. The results for the 0.3- and 1.6-ML films are summarized in Table III. One observes that the enhancement factor is indeed characteristic for each of the modes: The monolayer modes at 716, 781, and 808 cm^{-1} have identical enhancement factors for both layer thicknesses. Unfortunately, there is no clear relationship between modes in the first and second molecular layers, which makes it impossible to identify corresponding modes from their common enhancement factors. This is most likely related to the fact that together with the frequencies the respective cross sections are changed as well. In fact, the modes in the second layer consistently have significantly larger enhancement factors. This latter behavior can be understood if it is remembered that in the close vicinity of a metallic surface the scattering cross section of a perpendicular mode is fourfold increased by the image dipole. Apparently, this amplification is not any more fully effective even for molecules in the second layer, yielding a reduction in dipole scattering by 40 to 70% depending on the particular mode and hence to an increase of the enhancement factor. While this early weakening of the dipole enhancement may be surprising, it is fully consistent with the observation of the gradual breakdown of the surface selection rule for parallel modes starting as early as at 2- to 3-ML thicknesses (cf. Sec. IV).

B. C=O stretching modes

We now turn to the double peak at 1740/1771 cm^{-1}, which must be identified with the two IR active C=O

TABLE II. Comparison of those submonolayer modes of PTCDA/Ag(110), which are excited in the dipole scattering mechanism [cf. Fig. 4(c)] with perpendicularly polarized dipole active modes of the free D_{2h} molecule (representation B_{3u}, columns 2 and 3) and Raman active modes of the free D_{2h} modes of the free D_{2h} molecule [representation A_g^*, column 4, calculated; column 5, experimental peak positions in resonant Raman scattering of PTCDA films of H-passivated Si(111) substrates] (Ref. 26). Due to the reduction of the symmetry group rom D_{2b} to C_{2v} at the surface, both representations project onto the totally symmetric A_1 representation of C_{2v}. For more information see text. Theory II refers to the DFT calculation in the optimized tight-binding basis set.

HREELS submonolayer PTCDA Ag(110) (this work) (cm^{-1})	Theory II free molecule B_{3u} modes (this work) (cm^{-1})	HREELS multilayer (4.5 ML) PTCDA/Ag(110) (this work) (cm^{-1})	Theory II free molecule A_g modes (Scholz *et al.*, Ref. 26) and this work (Table I) (cm^{-1})	Experimental Raman shifts multilayer PTCDA/H/Si(111) (Scholz *et al.*, Ref. 26) (cm^{-1})
	36	44		
	174	196		
204	195	213		
			232	233
			383	389
			474	476
494	444	494		
			550	537
	531	572		
			639	624
			728	727
716	695	736		
781	769	810		
			863	858
808	818	867		
			1070	1054
			1140	1150
1231				
1259			1285	1305
			1304	1339
1325				
			1347	1381
			1393	1389
			1527	1544
1569			1616	1572
			1623	1590
			1723	1774

stretching vibrations. This doublet is present only in the multilayer. Because of the flat-lying adsorption geometry the absence of these *x* and *y* modes from the submonolayer *dipole spectrum* is indeed expected. However, there is a totally symmetric combination of stretch vibrations of the four terminal C=O groups, which could lead to a perpendicular dynamical dipole if the double-bonded oxygen atoms of the anhydride groups took part in the bonding of the PTCDA molecule to the surface: This bond would entail charge transfer perpendicular to the surface, and a sidewise motion of the oxygen atoms would then necessarily lead to a perpendicular redistribution of charge along these bonds, leading in turn to dipole activity even on a metallic surface. The fact that this mode is not seen in Fig. 4(c) and in the inset to Fig. 6 (the intensity in this frequency range is zero, not just small) could thus indicate that *the C=O groups are more realistically represented as being isolated from the surface, not taking part in the bonding*. While this conclusion is in agreement with photoemission results,[15] which show differential peak shifts indicative of bond formation predominantly for C-derived orbitals on the perylene skeleton, this first model is ruled out by the fact that even in the impact spectra of Fig. 4(b) the C=O stretch modes are missing. This points to the fact that in the submonolayer the C=O modes are *shifted* rather than just absent from the dipole spectrum.

In a second model, a *direct* interaction between the carbonyl O atoms and the Ag surface is supposed to take place, leading both to dipole activity and a frequency shift of the carbonyl stretching mode. Such a shift could, however, also be produced by an *internal* reorganization of molecular or-

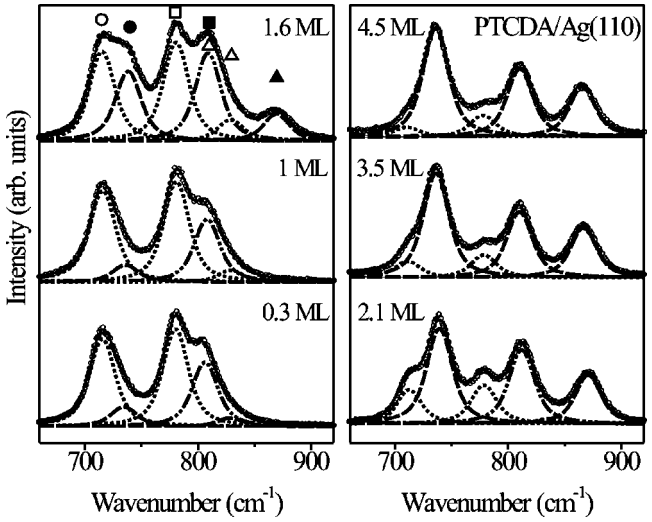

FIG. 7. Fitted spectra in the frequency range of the strongest z modes for various layer thicknesses. For more information on the fitting process see text. *Circles*: data points. *Solid lines*: fit to the data. *Dotted lines*: components belonging to the first monolayer (see text). *Dashed lines*: components belonging to the second and higher layers (see text). *Dashed-dotted lines*: component at 810 cm^{-1}, which is strong both in the submonolayer and multilayer regimes. The symbols in the 1.6-ML panel refer to symbols used in Figs. 8(a) and 8(b) for the respective component lines.

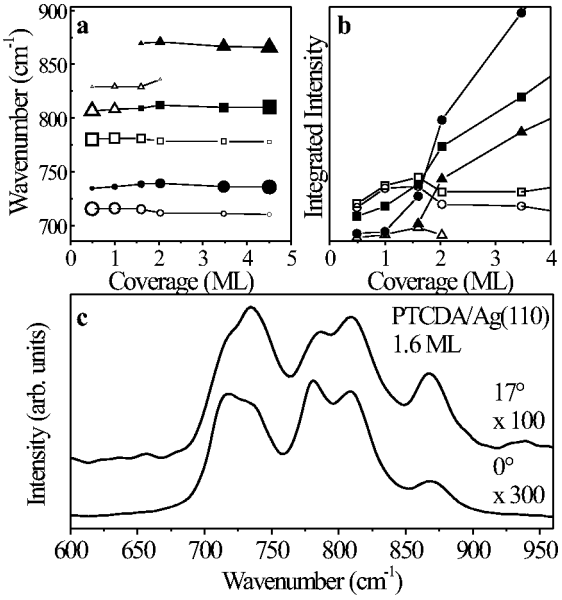

FIG. 8. (a) Frequencies of the fitted components of Fig. 7. During the fitting the frequencies were free fitting parameters. *Open symbols*, (sub)monolayer components; *full symbols*, components belonging to second or higher layers. The sizes of the symbols give qualitative measures of the respective intensities. (b) Integrated intensities of the component lines of Fig. 7. Symbols as in Fig. 7. (c) Comparison of the specular (0°) and off-specular (17°) spectra of a 1.6-ML layer. Magnification factors refer to the respective elastic peaks.

bitals as a result of the surface bonding of other molecular groups, e.g., the perylene core (third model). According to NEXAFS,[15,17] the bonding of PTCDA to the Ag surfaces mainly involves the perylene core of the molecule and not the anhydride groups. We thus prefer the third model to explain the shift of the carbonyl stretching modes. If the double-bonding character of the C=O bond is only slightly reduced through electron transfer from the surface to the molecule and eventually to the anhydride groups, large frequency shifts are expected, since the C-O stretch vibration is known to occur around 1000 cm^{-1}, namely, roughly 700 cm^{-1} lower than the C=O stretch frequency. It is just possible that the mode at 1569 cm^{-1} in the dipole spectrum [Fig. 4(c)] is in fact a shifted C=O stretch peak of A_g/A_1 symmetry. Indeed, the mode at 1569 cm^{-1} is reasonably close to the antisymmetric stretching mode of the carboxylate group COO^- (1556–1585 cm^{-1} for formate and acetate ions),[32] in which both oxygen atoms have identical bond order. The corresponding symmetric stretching mode occurs in the range 1351–1414 cm^{-1} (Ref. 32), again close to a measured peak at 1325 cm^{-1} only present in the submonolayer (Figs. 4 and 6). Of course, when discussing the modes at 1569 and 1325 cm^{-1} in terms of antisymmetric and symmetric carboxylate modes, one has to be aware that the displacements of the oxygen atoms have to be adjusted to the symmetry of the dianhydride groups of the given PTCDA molecule. In fact, such an adjustment seems possible if the oxygen bridges between the two carbonyl groups on either side of the molecule are maintained and the movement of the bridging O atom is supposed to take place parallel to the long (x) axis of the molecule. Depending on the phase relative to the in-phase bond stretching movement of the four terminal O atoms, this yields two totally symmetric modes with either predominant antisymmetric or symmetric C-O bond stretching character within the four COO groups of the molecule. According to this interpretation, the experiment thus presents evidence that the structure of the anhydride groups is strongly altered by the chemisorption, even though the bonding is mediated through the π electrons of the perylene core.

The interpretation of the modes at 1325 cm^{-1} and 1569 cm^{-1} given in this section contradicts the one implied by the inset to Fig. 6 and by Table II. However, we prefer the present explanation, mainly because a frequency shift of the breathing C=O stretch mode is strongly suggested by the lack of scattering intensity near 1770 cm^{-1} in the submonolayer impact spectra. As pointed out above, ultimately only calculations for the surface-bound molecule will yield an unambiguous solution.

TABLE III. Off-specular enhancement factors for the six strongest z modes, evaluated from HREELS spectra of two films, each recorded at 0° and 17° detection angle. Frequencies in lightface type correspond to the submonolayer species, frequencies in bold face correspond to molecules in the second layer. The mode at 830 cm^{-1} is weak and disregarded in the analysis. Further discussion can be found in the text.

Mode frequency (cm^{-1})	0.3 ML	1.6 ML
716	2.8	2.7
736		**4.5**
781	2.5	2.5
808/**810**	3.2	3.2/**3.5**
830	(5.0)	6.1
867		**7.5**

C. Low-frequency modes

We now turn our attention towards the low-frequency modes. For the (sub)monolayer, only one of the four predicted strong *z*-polarized modes (*38, 194, 222, 591* cm^{-1}) in the frequency region below 600 cm^{-1} appears. This is the mode at 204 cm^{-1} [see Fig. 4(c)]. Two additional structures in the monolayer spectrum, i.e., the modes at 237 cm^{-1} and the broad structure around 110 cm^{-1} are characteristic of the Ag(110) substrate. The latter corresponds to a residue of the Ag(110) surface phonon, which appears on clean substrates as a sharp peak at 105 cm^{-1}. The origin of the 237-cm^{-1} peak could possibly be CO_3. For the present Ag(110) single crystal it has been impossible to prepare the surface in such a way that this peak was absent. Finally, a very weak feature at 494 cm^{-1} is observed.

For the 572-cm^{-1} multilayer mode it is possible to give a plausible reason why it should indeed be strongly affected by the substrate. According to Fig. 5 and Table I, this mode is assigned to the long-axis folding-mode III at a calculated frequency of *591* cm^{-1} having 95% C character. The displacement pattern of this mode is shown in Fig. 9(a) on top of the Ag(110) surface. One sees that this mode is poorly fitted to the groove structure of the Ag(110) surface, which runs perpendicular to the node lines of this particular molecular vibration. Together with the strong involvement of the aromatic part of the molecule in this vibration, this misfit could provide an explanation for the absence of the 572-cm^{-1} peak from the (sub)monolayer spectra. The binding to the substrate via the aromatic system strongly modifies the relevant force constants and thus shifts the mode considerably in frequency. At the same time, the dipole activity may be drastically changed.

In fact, of the four *strong z* modes in the frequency range below 600 cm^{-1}, only one mode appears well fitted to the Ag(110) surface structure if the displacement patterns are evaluated. This is the mode appearing at *222* cm^{-1}. Its eigenvector reveals it as a short-axis folding mode (II) [Fig. 9(b)], which according to Fig. 5 and Table I has been assigned to the experimental frequency of 213 cm^{-1} in the multilayer. While it is experimentally impossible to distinguish whether it is the multilayer mode at 196 cm^{-1} or at 213 cm^{-1}, which belongs to the single monolayer mode at 204 cm^{-1}, it is very appealing from a theoretical point of view to associate the monolayer mode with the mode at 213 cm^{-1}, i.e., the short axis folding II because in that case this well-adapted mode would indeed be the *only* mode in the current frequency range, which is observed in the submonolayer regime. This assignment is supported by the fact that the shift of the *z* modes is generally occurring towards higher frequency in the multilayer (see, e.g., the modes at 736, 810, 867 cm^{-1}).

Given the fact that below 600 cm^{-1} only one of four strong *z* modes is observed in the (sub)monolayer, it is striking that the three modes at 716, 781, and 808 cm^{-1} (or 736, 810, and 867 cm^{-1} in the multilayer) are nevertheless present in spectra at *all* coverages and hence seem less susceptible to the presence of the surface. We note that the low-frequency *z* modes are characterized by in-phase displacements of atoms in large sections of the molecule with straight node-line patterns while the three upper modes at 736, 810, and 867 cm^{-1} in the multilayer (and to a certain degree the very weak mode at *492* cm^{-1}) consist of localized distortions in which neighboring atoms tend to move in opposite directions. These modes also tend to have concentric node lines. If the bonding to the substrate is affected by the delocalized π system, then it seems quite natural that displacements involved in the latter modes will not strain the bond between molecule and substrate to such a degree as the former. As a result, the intramolecular force constants remain the frequency determining ones, yielding only small shifts and small changes in dipole activity.

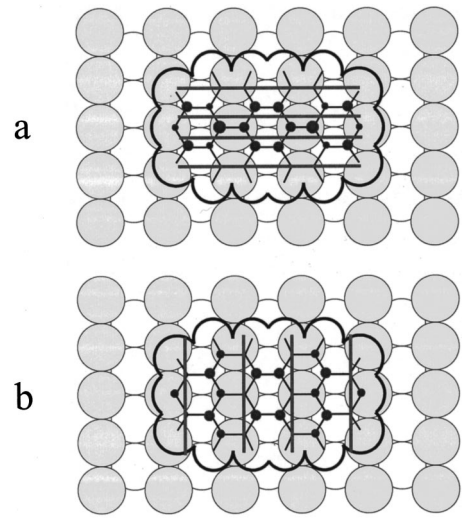

FIG. 9. Schematic representation of the eigenvectors of two calculated vibrational modes of the free PTCDA molecule. (a) Long-axis folding-mode III calculated at 534 cm^{-1}; (b) short-axis folding-mode II calculated at 196 cm^{-1}. The molecule is shown in its proper adsorption site on the Ag(110) surface.[13] Light gray Ag atoms are above the plane of paper, white Ag atoms beneath it. The molecule is represented by its bonds (black lines) and its border line (van der Waals radii of the atoms on the periphery). Straight gray lines represent node lines of the atomic movements. Atoms moving perpendicular to the plane of paper are represented by circles, the size being a qualitative measure of the respective amplitudes.

Finally, we discuss the submonolayer mode at 494 cm^{-1}. Two explanations are conceivable for this mode. First, it could be related to the multilayer mode at 572 cm^{-1} as its frequency-shifted counterpart. In this particular case, the frequency shift of 78 cm^{-1}, though having the right direction, would be rather larger as compared to the other modes. This unusually large shift could, however, be due to the strong misfit of this mode to the surface, which was already pointed out. Alternatively, this peak could be related to the weak mode predicted at *492* cm^{-1}. The fact that even for 4.5 ML a distinct structure appears at this frequency both in the as-measured spectrum of Fig. 6 and in the resolution-enhanced spectrum of Fig. 5 is clearly in favor of this latter explanation.

VII. CONCLUSION

In this paper we have shown that vibrational spectroscopy can be used to great advantage to investigate the interaction at the interface of a thin organic molecular film with a single crystalline surface if the employed spectroscopy is sufficiently surface sensitive. Our results show that HREELS

clearly fulfils this prerequisite. The spectra thus gained can serve as vibrational fingerprints of the molecular structure of an organic film. In this way it has been possible to relate spectral features to structural properties of thin PTCDA films on Ag(110). Moreover, the vibrational data in principle supply microscopic information about the binding interaction between the substrate and the organic adlayer. This information can best be extracted with the aid of theoretical calculations of the molecular vibrational modes as the large number of atoms per molecule provides a vast number of IR active modes that are otherwise difficult to assign. The multilayer spectra that have been presented correspond very well with our theoretical calculations for the free molecule, except for small frequency splittings detectable in FTIR due to intermolecular interactions. In contrast, the monolayer spectra require calculations of the *surface-bound* molecule before they can be unambiguously interpreted. For this reason, the present *vibrational* experiments have not yet revealed the nature of the bonding of PTCDA to the silver substrate in detail. It is apparent, however, that both the perylene core of the molecule and the anhydride groups are strongly modified by the bonding, as vibrational modes located on either of the two are strongly affected.

We wish to close this paper with an outlook on further work, which is currently in progress. While it is generally true that the strength of the molecule substrate interaction determines to a larger extent the ensuing surface order, there are indications that also the intermolecular interaction plays an important role in determining the structural properties of ultrathin organic films. The arrangement of quadrupolar PTCDA molecules in the herringbone pattern may serve as an example. Naturally, the role of these molecule-molecule interactions will be greater for films in which the molecules are more densely packed. For this reason, we have also investigated the Ag(111) surface,[33] where a different lateral order is realized. Already the first monolayer grows in the structure of the (102) plane of the PTCDA bulk structure, which is denser than the brick-wall structure on Ag(110).[7] Apparently, in this case the interaction between the surface and the molecule is considerably weaker such that no substrate-induced structure change takes place. It is instructive to compare vibrational spectra for both surfaces, and one finds that the anticipated differences with respect to both the molecule-molecule and the molecule-substrate interaction lead to drastic differences in the submonolayer spectra.[33]

Second, it is also possible to extend the present experiments by taking advantage of the fact that any HREEL spectrometer can also be used for energy loss spectroscopy in the loss range of electronic transitions. It is thus possible to investigate vibrational and electronic loss spectra on the same films. This yields a unique correlation thereby of the structural and electronic film properties for ultrathin films,[34] which is promising since it is mostly the electronic and optical properties one is interested in for possible applications.

ACKNOWLEDGMENTS

We would like to acknowledge fruitful discussions with N.V. Richardson, University of St. Andrews, U.K. Financial support by the DFG through Project No. So407 is also acknowledged. One of us (E.U.) thanks the Fonds der Chemischen Industrie for financial support.

*Author to whom correspondence should be addressed: Dr. Stefan Tautz, Institut für Physik, Technische Universität Ilmenau. Fax: +49 (0)3677 693205. Electronic address: tautz@physik.tu-ilmenau.de

[1] G. Horowitz, F. Garnier, A. Yassar, R. Hajlaoui, and F. Kouki, Adv. Mater. **8**, 52 (1996).
[2] T. N. Jackson, Y. Y. Lin, D. J. Gundlach, and H. Klauk, IEEE J. Sel. Top. Quantum Electronics **4**, 100 (1998).
[3] G. Gu, V. Bulovic, P. E. Burrows, S. R. Forrest, and M. E. Thompson, Appl. Phys. Lett. **68**, 2606 (1996).
[4] P. E. Burrows and S. R. Forrest, Appl. Phys. Lett. **64**, 2285 (1994).
[5] T. N. Jackson, Y. Y. Lin, D. J. Gundlach, and H. Klauk, IEEE J. Sel. Top. Quantum Electron. **4**, 100 (1998).
[6] E. Umbach, M. Sokolowski, and R. Fink, Appl. Phys. A: Mater. Sci. Process. **63A**, 565 (1996).
[7] K. Glöckler, C. Seidel, A. Soukopp, M. Sokolowski, E. Umbach, M. Böhringer, R. Berndt, and W.-D. Schneider, Surf. Sci. **405**, 1 (1998).
[8] C. Seidel, C. Awater, X. D. Liu, R. Ellerbrake, and H. Fuchs, Surf. Sci. **371**, 123 (1997).
[9] E. Umbach, K. Glöckler, and M. Sokolowski, Surf. Sci. **402**, 20 (1998); **404**, 31 (1998).
[10] C. Seidel, J. Poppensieker, and H. Fuchs, Surf. Sci. **408**, 223 (1998).
[11] C. Kendrick, A. Kahn, and S. R. Forrest, Appl. Surf. Sci. **104/105**, 586 (1996).
[12] T. Schmitz-Hübsch, T. Fritz, F. Sellam, R. Staub, and K. Leo, Phys. Rev. B **55**, 7972 (1997).
[13] M. Böhringer, W. D. Schneider, K. Glöckler, E. Umbach, and R. Berndt, Surf. Sci. Lett. **419**, L95 (1998).
[14] L. Kilian, M. Sokolowski, and E. Umbach (unpublished).
[15] J. Taborski, P. Väterlein, H. Dietz, U. Zimmermann, and E. Umbach, J. Electron Spectrosc. Relat. Phenom. **75**, 129 (1995).
[16] M. Jung, U. Baston, G. Schnitzler, M. Kaiser, J. Papst, T. Porwol, H.-J. Freund, and E. Umbach, J. Mol. Struct. **293**, 239 (1993).
[17] E. Umbach, C. Seidel, J. Taborski, R. Li, and A. Soukopp, Phys. Status Solidi B **192**, 389 (1995).
[18] M. P. Shea and W. A. Dench, Surf. Interface Anal. **1**, 2 (1979).
[19] A. J. Lovinger, S. R. Forrest, M. L. Kaplan, P. H. Schmidt, and T. Venkatesan, J. Appl. Phys. **55**, 476 (1984).
[20] M. Möbus, N. Karl, and T. Kobayashi, J. Cryst. Growth **116**, 4951 (1992).
[21] M. L. Kaplan, C. S. Day, A. J. Lovinger, P. H. Schmidt, and S. R. Forrest (private communication).
[22] K. Akers, R. Aroca, A.-M. Hor, and R. O. Loutfy, J. Phys. Chem. **91**, 2954 (1987).
[23] B. G. Frederick, G. L. Nyberg, and N. V. Richardson, J. Electron Spectrosc. Relat. Phenom. **64/65**, 825 (1993).
[24] B. G. Frederick, B. B. Frederick, and N. V. Richardson, Surf. Sci. **368**, 82 (1996).
[25] M. Elstner, D. Porezag, G. Jungnickel, J. Elsner, M. Haugk, Th. Frauenheim, S. Suhai, and G. Seifert, Phys. Rev. B **58**, 7260 (1998).
[26] R. Scholz, A. Yu. Kobitski, T. U. Kampen, M. Schreiber, D. R. T. Zahn, G. Jungnickel, M. Elstner, M. Sternberg, and Th. Frauenheim, Phys. Rev. B **61**, 13 659 (2000).

[27] M. Frisch, GAUSSIAN 98, *Rev. A6* (Gaussian, Inc., Pittsburgh, PA, 1998).
[28] A. D. Becke, J. Chem. Phys. **98**, 5648 (1993).
[29] M. Murakami, S. Iijima, and S. Yoshimura, J. Appl. Phys. **60**, 3856 (1986).
[30] H. Kamo, M. Yudasaka, S. Kurita, T. Matsui, R. Kikuchi, Y. Ohki, and S. Yoshimura, Synth. Met. **68**, 61 (1994).
[31] H. Fuchigami, S. Tanimura, Y. Uehara, T. Kurata, and S. Tsunoda, Jpn. J. Appl. Phys., Part 1 **34**, 3852 (1995).
[32] K. Nakamoto, *Infrared Spectra of Inorganic and Coordination Compounds* (Wiley, New York, 1963).
[33] F. S. Tautz, S. Sloboshanin, V. Shklover, R. Scholz, M. Sokolowski, J. A. Schaefer, and E. Umbach, Appl. Surf. Sci. (to be published).
[34] V. Shklover, F. S. Tautz, S. Sloboshanin, R. Scholz, M. Sokolowski, J. A. Schaefer, and E. Umbach, Surf. Sci. (to be published).